This is a repository copy of *Preparation of Sodium-Activated Natural Bentonite Clay Incorporated Cellulose Acetate Nanofibres by Free Surface Electrospinning and Its Proposed Applications*.

White Rose Research Online URL for this paper:
http://eprints.whiterose.ac.uk/137256/

Version: Accepted Version

Book Section:

Chapter

Preparation of Sodium-Activated Natural Bentonite Clay Incorporated Cellulose Acetate Nanofibres by Free Surface Electrospinning and Its Proposed Applications

Mohamed Basel Bazbouz[*], PhD
Textile Technology Research Group, School of Design,
University of Leeds, Leeds, UK

Abstract

Incorporating activated bentonite clay (BC) into electrospun nanofibres is an established strategy for modulating adsorption behaviour. In the present study, we have provided a comprehensive review of electrospun nanofibres from different types of polymers with synthesized

---
[*] Corresponding Author Email: m.b.bazbouz@leeds.ac.uk.

montmorillonite clays (MMT). Loading activated natural bentonite clay (BC) into any type of polymer can improve the adsorption property of electrospun nanofibres, but BC must be well dispersed, suspended and loaded to achieve any benefit. Naturally occurring calcium BC was completely activated to sodium BC with a 4 wt.% sodium carbonate (Na_2CO_3)/BC ratio. High throughput composite nanofibrous fabrics were produced from cellulose acetate (CA)/BC spinning solutions using free surface electrospinning and the effect of BC loadings on viscosity, surface tension and electrical conductivity prior to spinning were studied. It has been found that the higher the BC loading rate and thus higher viscosity and surface tension, the higher the applied voltage and the lower the rotation speed of the wires electrode were required in order to get the highest productivity accompanied with electrospinning stability. Chemical and thermal analyses were conducted on as-spun fibres, and SEM and TEM revealed a nanofibrous morphology consisting of an inter-penetrating network of fibres and semi-spherical features resembling jellyfish with an internal core of BC. The problem with the existing adsorption process and the need for the change in the texture of the separation layer that controls the performance of the resultant membrane in terms of flux and selectivity were discussed and directed. We believe that this study may pave the way for further use of electrospun nanofibres loaded with clay in a wide variety of environmental and medical applications.

Keywords: free surface electrospinning, nanofibres, bentonite clay, cellulose acetate, montmorillonite, composite

INTRODUCTION

Electrospun polymer nanofibres have interesting characteristics resulting from their sub-micron diameter, fine interconnected porous network and high surface to weight ratio compared to other fibrous structures [1]. These characteristics promote enhanced surface reactivity and make nanofibres attractive for numerous applications such as air and liquid filtration [2], reinforced composites [3], and medical devices [4]. For most engineering and industrial applications of nanofibres, thermal stability and mechanical stability are normally required [5] and both can be

addressed by incorporation of nanometre-sized components such as metallic nanoparticles [6], carbon nanotubes (CNT) [7] and single or hybrid aluminous silicate clay fillers [8-51].

It has been demonstrated that electrospinning of polymer-clay composites with a small amount (1-10 wt.%) of clay filler can lead to remarkable improvements in wettability and swelling [42], mechanical properties, including Young's modulus [19, 24], thermal stability [49], flame retardancy [20], heat distortion temperature [45], UV resistance [25], chemical affinity [33] and gas barrier properties [40] compared to pure polymer nanofibres. BC, formed from weathering of volcanic ash in the presence of water, is an absorbent aluminium phyllo silicate clay consisting mostly of smectite [52]. Owing to its adsorptive and absorptive capabilities and cation exchange capacity, it has been applied in healthcare for a variety of purposes including wound healing and infection control [53-55], skin protection [56], cosmetics [57] and rheumatism treatment [58]. Moreover, BC has been applied in heavy metal ion adsorption [59] and removal of organic pollutants from water [60]. BC based on the dominant exchangeable cations present, is referred to as either calcium, sodium or potassium bentonite [61, 62]. The smectite group such as montmorillonite (MMT) is the most dominant mineral in bentonite, representing up to 70-80% by weight, while other minerals in bentonite such as kaolinite and none-clay minerals make up to 20-30% [62]. Single or hybrid MMT with or without modification has been successfully synthesised and electrospun with different polymers. Table 1 summarises the electrospun nanofibres produced with single or hybrid MMT fillers and their proposed applications [8-51].

The incorporation of activated, natural BC in electrospun fibres has received substantially less attention than synthesised materials in the literature, particularly so using electrospinning methods that utilise free surface methods. Electrospinning is typically restricted to 0.1-1.0 g.hr^{-1} for a single spinneret [63], with a polymer solution throughput in the range of 0.1 to 10 ml.hr^{-1}[64]. To increase yield, numerous needle-free electrospinning approaches have been developed [65-67], some of which

involve the rotation of a solid surface through a polymer solution. One example is the Nanospider®[68] in which the polymer solution is electrospun from either wire-based or roller electrodes, so that nanofibre production rate can be conveniently adjusted depending on the electrode width, the linear speed of the wires/roller and the number of spinning heads placed in series [66, 68, 69]. Fibres with diameters in the range 50 - 500 nm can therefore be produced at a rate of about 1.5 g.min^{-1} per meter of roller length [68].

Given the dearth of previous studies focusing on the preparation of nanofibres containing natural BC, the purpose of this study is to determine the feasibility of delivering such composite fibres by means of high speed, free surface electrospinning. In the present investigation, CA was selected as a carrier polymer because of its ease of solubility in organic solvents, chemical resistance and thermal stability [70, 71]. The chemical and physical properties of the resulting materials were also studied to understand the extent to which incorporation of the natural BC modulated behaviour.

MATERIALS AND METHODS

Materials

Cellulose acetate CA (39.8% acetyl content, MW of 30.000 g.mole^{-1}), sodium carbonate (Na$_2$CO$_3$), carboxymethyl cellulose (CMC), hydrochloric acid (HCl) (reagent grade, 37%), acetic acid (AcOH) (99 - 100%) and sulphuric acid (95-98% H$_2$SO$_4$) were purchased from sigma Aldrich (UK). Natural bentonite clay (Beloon) (BC), was collected during the dry season from Azaz, northwest of Aleppo, Syria (Latitude: 36°35'11"N, Longitude: 37°02'46"E).

Table 1. Electrospun nanofibres from different polymers with MMT fillers and their proposed applications

Polymer system	Polymer name	Single or hybrid clay fillers –with or without modification	Polymer solution – nanofibre/clay characterisations	Suggested applications by the reference authors.	Ref.
Single polymer	Nylon 6	MMT	DSC, SEM, TEM, WAXRD.	--------------------	[8]
	Nylon 6	O-MMT	VIS, SEM, TEM, WXRD, DSC, TGA, MP.	High-performance filters and fibre reinforcement materials.	[9]
	Nylon 6	O-MMT	VIS, ST, SEM, AFM, TEM, DWA.	Water adsorption.	[10]
	Nylon 6	(O-MMT) with Fe_2O_3 Sputter coating	SEM-EDX, AFM, XPS, TGA.	Functional materials.	[11]
	Nylon 6	Fe-OMT	TGA, HREM, SEM, XRD, LR.	--------------------	[12]
	Nylon 6	Synthesized Fe-OMT	FTIR, XRD, HREM, SEM-EDX, TGA.	--------------------	[13]
	Nylon 6	MMT, O-MMT	TGA, DSC, SEM, AFM, XRD.	--------------------	[14]
	Nylon 6	Synthesized Fe-OMT with Magnetron sputter coating	HREM, SEM-EDX, AFM, XPS, TGA, FP.	Fire protective fabrics.	[15]
	Nylon 6	MMT clay	SEM, TEM, EDX, XRD, MP, BP, MA, LP, MG.	Coated packaging films against oxygen and moisture.	[16]
	Nylon 6	MMT clay	TGA, SEM, TEM, CC.	Fire protective clothing.	[17]
	Nylon 6	O-MMT	VIS, EC, ST, WAXRD, SEM, TEM.	--------------------	[18]
	Polyacrylonitrile (PAN)	Na-MMT nanocomposites	XRD, TEM, SM.	--------------------	[19]
	PAN	Synthesized Fe-OMT	XRD, TEM, SEM, TGA, FP, MP.	Fire protective fabrics.	[20]
	PAN	Sodium activated (Na - MMT)	SEM, TEM, XRD, TGA.	--------------------	[21]

Table 1. (Continued)

Polymer system	Polymer name	Single or hybrid clay fillers –with or without modification	Polymer solution – nanofibre/clay characterisations	Suggested applications by the reference authors.	Ref.
	PAN	Hexadecyl trimethyl ammonium bromide (CTAB) modified MMT (MMT/GO)	SEM, AFM, TEM, XRD, TGA, MP.	As nanofillers.	[22]
	PAN	Synthesized Na-MMT	SEM, WAXRD, TGA, IEP.	Environmental protection.	[23]
	Cellulose Acetate (CA)	MMT	VIS, EC, TGA, DTG, XRD, MP, SEM, EF-TEM, EDX.	---------------------	[24]
	CA	O-MMT	SEM, TEM, UV-S.	Enzyme immobilization.	[25]
	Cellulose extracted from corn.	Na - MMT	XRD, FTIR, VIS, SEM, DSC.	---------------------	[26]
	CA	Anion surfactant/MMT	SEM, FTIR, DSC, TGA, XRD, HMA.	Heavy metal adsorbent in water treatment.	[27]
	PVA	MMT	FE-SEM, XRD, TGA, MP.	---------------------	[28]
	MMW-PVA, HMW-PVA	MMT	VIS, FE-SEM, TEM, TGA, MP.	---------------------	[29]
	PVA	MMT/Ag Nanoparticles	FE-SEM, TEM, XRD, TGA, AP.	Antibacterial applications.	[30]
	PVDF	Na - MMT	WAXRD, FTIR, DSC, TEM, SEM, VIS.	---------------------	[31]
	PVDF	MMT	Crystallization kinetics	---------------------	[32]
Polymer system	Polymer name	Single or hybrid clay fillers – with or without modification	Polymer solution – nanofibre/clay characterisations	Suggested applications by the reference authors.	Ref.
	PVDF	MMT	FE-SEM, P, EU, DSC, FTIR, IC.	Separators for lithium-ion batteries.	[33]
	PU	O-MMT	WAXRD, SEM, TEM, EC, MP.	---------------------	[34]

Polymer system	Polymer name	Single or hybrid clay fillers –with or without modification	Polymer solution – nanofibre/clay characterisations	Suggested applications by the reference authors.	Ref.
	PU	Chlorhexidine acetate drug (CA)/MMT	SEM, XRD, CAM, P, AP, DRM.	Topical drug delivery application.	[35]
	PLA	Synthesized MMT	SEC, DSC, TGA, TEM, WAXRD, FTIR, PM.	Gas barrier for food packaging applications	[36]
	PLLA	MMT	SEM, XRD.	Engineered scaffold applications	[37]
	Silk Fibron	MMT	SEM, FESEM, TEM, FTIR- XRD.	Scaffold for tissue engineering	[38]
	Levan	Na - MMT	UV-S, SLS, DLS, WAXRD, TGA, DSC, FTIR, MP.	Cosmetics and pharmaceutical coatings.	[39]
Blends of polymers	PLA/Keratin	Na - MMT	VIS, EC, SEM, TEM, ATR–FTIR, DSC, FPT.	Volatile organic compounds (VOCs) removal filters from.	[40]
	Pullulan/PVA	MMT	SEM, TEM, FTIR, XRD, TGA, MP.	--------------------	[41]
	Pullulan/PVA	MMT	FE-SEM, TEM, XRD, TGA, WAM, WRM, MP.	Personal hygiene products.	[42]
	PVA/PVDF	O-MMT	SEM, FTIR, TGA, MP, IC, CV.	Lithium ion batteries	[43]
	PVA/ Chitosan	MMT	FE-SEM, XRD, TEM, MP, TGA.	Reinforcement in matrix.	[44]
	PVA/PVP	Octadecyl amine (ODA)-MMT	FTIR, XRD, FE-SEM, TEM, EDX, TGA, DSC, EC, TR.	Electrically conductive nanomaterials.	[45]
	PVA/Poly (VP-alt-MA)	(ODA)-MMT + silver (Ag)			
	PVA/Poly(MA-alt-MVE)	(ODA)-MMT	FTIR, XRD, FE-SEM, EDX, CVMS.	Power, electrochemical and fuel cell nanotechnology.	[46]
	PVA/Poly (maleic acid-alt-acrylic acid)	(ODA)-MMT + Ag	FTIR, XRD, SEM, TGA, DSC, EC, TR, CVMS.	Electrically conductive nanomaterials.	[47]

Table 1. (Continued)

Polymer system	Polymer name	Single or hybrid clay fillers –with or without modification	Polymer solution – nanofibre/clay characterisations	Suggested applications by the reference authors.	Ref.
Co-polymers	PVA/Poly (itaconic anhydride-alt-2-vinyl, 1,3 dioxalan)	(ODA)-MMT + Ag	FTIR, XRD, FE-SEM, TGA, DSC, EC, TR, CVMS.	Microelectronics, Nano lithographical technology and semiconductors.	[48]
	Poly(MMA-CO-MAA)	Synthesized Na-MMT	SEM, TEM, WAXRD, TS, DLSM, PSR.	---------------------	[49]
	PCL and G-PLA	(ODA)-Na- MMT + Ag	FTIR, SEM-EDX, FE-SEM, TEM, TGA.	Biomedical applications	[50]
	Poly(Vinyl Alcohol- co-Vinyl Acetate)	(ODA)-MMT + Ag	XRD, FE-SEM,AAT	Food, bioengineering and Nano-engineering processing.	[51]

Abbreviations: (O-MMT): Organically Modified Montmorillonite, (Fe-OMT): Organic-Modified Iron-Montmorillonite, (DWA): Dynamic Water Adsorption, (XPS): X-Ray Photoelectron Spectroscopy, (FE-SEM): Field Emission Scanning Electron Microscope, (HREM): High-Resolution Electron Microscopic, (LR): Laser Raman Spectroscopic, (XRD): X-Ray Diffraction, (WAXRD): Wide Angle X-Ray Diffraction, (MP): Mechanical Properties, (FP): Flammability Property, (EDX): Energy Dispersive X-ray, (BP): Barrier Properties, (MA): Moisture Absorption, (LP): Lipid Peroxidation, (MG): Microbial Growth, (CC): Combustion Characteristics, (EC): Electrical Conductivities, (ST): Surface Tension, (DTG): Derivative Thermogravimetric, (FE-TEM): Field Emission Transition Electron Microscope, (FTIR): Fourier Transform Infrared Spectroscopy, (ATR–FTIR): Attenuated Total Reflectance–Fourier Transform Infrared Spectroscopy, (DSC): Differential scanning calorimetry, (UV-S): Ultraviolet Visible Spectrophotometry, (SM): Storage Modulus, (IEP): Ion Exchange Properties, (AP): Antimicrobial Performance, (P): Porosity, (EU): Electrolyte Uptake, (CAM): Contact Angle Measurement, (DRM): Drug Release Measurements, (SEC): Size Exclusion Chromatography, (PM): Permeability Measurements, (SLS): Static Light Scattering, (DLS): Dynamic Light Scattering, (WAM): Water Absorbency Measurement, (WRM): Water Retention Measurement, (FPT): Filtration Performance Tests, (IC): Ionic Conductivity, (CV): Cyclic Voltammetry, (TR): Thermal Resistance, (CVMS): Current–Voltage Measurement System, (TS): Thermal Stability, (DLSM): Dynamic Light Scattering Measurement, (PSR): Polymer Solution Rheology, (AAT): Antifungal and Antimicrobial Testing, (TGA): Thermogravimetric Analysis, (HMA): Heavy Metal Absorption.

BC Purification and Activation

BC was initially dried in ambient conditions, followed by oven drying at 100°C for 24 h to remove moisture from the clay. Dried BC was crushed, ground and sieved using a 63 μm mesh. Purification of BC involved immersing 100 g of BC in 200 ml of 1.6 M HCl and stirring for 4 h at 100 r min^{-1} then the BC was filtered and washed in distilled water. The resulting purified BC was heated and dried at a temperature of 100°C for 6 h. In order to activate the purified BC with sodium Na$^+$ (referred to as "Na$^+$ sodium ion exchange activation"). 4 wt.% of Na$_2$CO$_3$ was added to the BC and stirred for 2 h to allow for both sodium ion exchange and water to remove the exchanged calcium. Finally, the purified and activated BC was dried at a 100°C for 24 h in readiness for loading in to the CA solution.

Chemical Analysis of BC

The chemical components of the raw BC, purified BC after reaction with HCl, and activated BC after reaction with Na$_2$CO$_3$ were measured using atomic absorption spectroscopy (AAS; PYE Unicam SP191, Cambridge, UK). The AAS was calibrated while solutions of the clay samples were prepared. In brief, 1 g of each clay sample was dissolved in 10 ml of H$_2$SO$_4$ while stirring for 3 h, then the degree of absorption was calculated. Clay samples were then filtered and small quantities of the filtrates were collected and diluted in a 250 ml of water. Finally, AAS was used to determine each clay component using a N$_2$O-Acetylene flame, and a hollow cathode lamp to calculate the proportion of each component [72, 73].

Fabrication of CA/BC Composite Nanofibrous Fabrics

A predetermined amount of BC with 4 wt.% CMC was mixed and added to hot aqueous AcOH (75:25, v/v) while stirring magnetically at 300

r min^{-1} at room temperature for up to 2 h. In parallel, CA was dissolved in aqueous AcOH (75:25, v/v) at concentrations of 15% (w/v) whilst stirring with 300 r min^{-1} at 70°C for to 5 h. The CA/BC solutions were blended with a 5, 10, 15, 20, 25 wt.% of BC (with respect to the weight of CA) and CA solution while stirring magnetically at 300 r min^{-1} at room temperature for up to 24 h. Samples nomenclature is coded in this work in the form of 'CA15BCX' which refers to a CA solution at 15% (w/v) concentration, where 'X' indicates the concentration of BC wt.%. The CA/BC composite nanofibres from each spinning solution is referred to as CA15BC0, CA15BC5, CA15BC10, CA15BC15, CA15BC20, CA15BC25, respectively. Nanofibrous fabrics from the CA/BC blends were electrospun using a NS LAB 200 Nanospider electrospinner, (Elmarco, Czech Republic) using the four wire electrode. The applied voltage and working distance were 65-75 kV and 12 cm, respectively. The rotation speed of the electrode was 1-2 r min^{-1} and the linear speed of the collector was 10 cm.min^{-1}. Fibres were deposited on to a spunbond polypropylene (PP) nonwoven fabric containing fibres of 3 ± 0.30 denier. The environmental temperature was 23±2 °C and the relative humidity was 30%. The as-spun fibre webs were dried for at least 3 days at room temperature.

Viscosity, Surface Tension and Electrical Conductivity Measurements

The viscosities of CA/BC solutions were measured on a Brookfield digital viscometer (Brookfield DV-II Viscometer, USA). Readings were taken at 23±2°C using a spindle and chamber SC4-25/13R. CA/BC solutions volume of 16.1 mL for each sample was placed in a beaker, into which the spindle of the viscometer was immersed and rotated at a shear rate in the range from 60 to 1 rpm (equivalent to 1-0.017 sec^{-1} in order to characterise the rheological properties of the CA/BC solutions.

The surface tension of the CA/BC solutions was analysed by means of the pendant drop method using a CAM 200 contact angle goniometer (KSV Instruments Ltd., Helsinki, Finland). A pendant drop method in six

parallel measurements using a micro-syringe with an automatic dispenser and a CCD fire wire camera (512x480) with telecentric zoom optics combined with LED based background lighting allowing capturing images at frame intervals from 10 ms to 1000s was carefully conducted. Each sample was analysed in triplicate and the mean values of the triplicates were plotted. The surface tension γ was calculated by using the equation;

$$\gamma = \frac{g.\rho.d_e^2}{S_f} \tag{1}$$

where g is the acceleration of gravity, ρ is the difference in density of the air and the solution, de is the equatorial diameter of the droplet and S_f is the shape factor, as referenced in [74].

Electrical conductivity of CA/BC solutions was examined by Novocontrol broadband dielectric impedance spectrometer (Germany), with integrated alpha-A high performance frequency analyser in 0.1 Hz to 10 MHz frequency. Samples were tightened by using vacuum sealed parallel electrodes (diameter of 18 mm) as a specimen holder cell with a spring for sealing out the air and the data was analysed by using WinFit software. Measurements were carried out at a temperature of 23±2°C and the spectrometer was set to a bias of 1 volt and were measured between frequency sweeps of 1.0 Hz to 1.8 MHz.

Scanning Electron Microscopy (SEM) and Energy Dispersive X-Ray Spectroscopy (EDX)

The 2D surface morphology of the BC and the fabric structure of the CA/BC nanofibres were observed by SEM (Hitachi S-2600N, Japan) with a secondary electron detector. Samples were sputter coated with high resolution sputter coater (Emitech K550X, UK) with gold layers under high vacuum. An acceleration voltage of 3-5 kV was used with a working distance of 5.3-11.0 mm. Images were captured at magnifications in the range of 70x to 30000x. The average fibre diameters in each sample were

estimated by evaluating a minimum of 50 fibres from different regions of the sample. The average electrospun CA nanofibre diameters were measured from multiple SEM images by means of image analysis software (SemAfore 5.21, JEOL CO., Finland) with at least 50 measurements per image to determine mean fibre diameter and associated frequency distributions. Values were expressed as mean ± standard error. In order to analyse the elemental components presented in the clay such as silicon and iron, etc., EDX spectrum with Oxford instruments Aztec energy EDS analysis software and 80 mm X-Max SDD detector were applied.

Transmission Electron Microscopy (TEM) and Nanoscale EDX Mapping

TEM (FEI Titan3 Themis 300, FEI^{TM} Netherland) and nanoscale EDX elemental quantitative mapping (FEI Super-X 4-detector EDX system) were used to confirm coexistence and to determine the size distribution and structure of the BC within the nanofibres. CA/BC nanofibres were collected onto carbon coated grids with a 300 mesh. Images were taken at an acceleration voltage of 300 KV.

Structure and Thermal Analysis of CA/BC Composite Nanofibrous Fabrics

A wide angle X-ray diffraction (WAXD, Bruker AXS D8 advanced, Germany) analyses were carried out in order to study the structural properties of BC and CA/BC composite nanofibres. Samples were scanned under conditions as the following scanning angle between $2\theta = 2°$ and $60°$ under room temperature, wave length of the X-ray beam of 0.154018 nm (Cu Ka anode and cathode radiation), a scan speed of $1°$ degree.min^{-1}, working voltage of 40 kV and working current of 40 mA.

Thermal analyses of BC and CA15BC0, CA15BC5 and CA15BC10 electrospun composite nanofibres which include mass loss wt.% and heat

flow ($W.g^{-1}$) as a function of heating temperature were conducted by using thermogravimetric analyser & differential scanning calorimeter (TGA/DSC 1 Star system, Mettler Toledo, Switzerland). A heating temperature of 40 - 600°C and a heating rate of $10°C.min^{-1}$ in nitrogen with flow rate of 50 $cm^3.min^{-1}$ were applied. Specimen weights of 2-10 mg were applied.

RESULTS AND DISCUSSION

Purification, Activation and Suspension of BC

The BC mineral composition mainly comprises smectite groups such as montmorillonite, beidellite, saponite and hectorite with impurities such as dolomite and illite [75]. Table 2 gives the measured chemical compositions of the raw, purified and activated BC, which includes metals oxides such as SiO_2, Al_2O_3, Fe_2O_3, MgO, CaO, Na_2O and TiO_2, water and carbon dioxide CO_2. The origin of CO_2 in the raw clay is due to dissociation of calcium carbonate or magnesium carbonate [76]. Purification can be achieved with HCl [77]. It is apparent from the compositions of purified BC treated with HCl that CO_2 is effectively removed. In addition, HCl purified BC has greater SiO_2, Al_2O_3 and Fe_2O_3 content than untreated BC.

Table 2. Chemical composition (wt.%) of raw,
HCl purified and Na_2CO_3 activated BC

Materials	SiO_2	Al_2O_3	Fe_2O_3	MgO	CaO	CO_2	H_2O	Na_2O	TiO_2	Sum
Raw BC	46.6	14.4	7.2	6.7	5.8	6.2	12.8	0.13	0.16	99.99
HCl purified BC	53.5	16.5	7.9	4.5	2.2	------	14.8	0.08	0.13	99.61
Na_2CO_3 activated BC	51.8	16.6	7.8	4.3	2.16	1.37	13.6	2.1	0.13	99.86

Calcium BC was completely converted to sodium BC when the clay was activated by Na_2CO_3 at (2.5-5%) ratio [78, 79]. Hence, Na^{+1} smectite clay is one of the preferred layered materials for the preparation of nanocomposites because of its high cation exchange capacity, high surface area, strong adsorption /absorption capacities within their interlamillar spaces and thus swelling capacity [80]. It is clear from the compositions of activated BC with Na_2CO_3 that Ca^+ ions were exchanged by Na^+ ions where Na_2O became 2.1% after it was 0.13% when 4 wt.% of Na_2CO_3 was added. However, in addition to the purification and activation achieved, the HCl and Na_2CO_3 treatments partially altered the morphological structure of the clay which will be clarified hereinafter.

We believe that the main challenge for processing composite nanofibres at the present time is to improve the dispersion and suspension of the BC particles in the polymer solution for enhancing the morphological uniformity of the electrospun nanofibres. It has been reported that activation of bentonite clay with Na_2CO_3 (increasing the (Na^+/Ca^{+2} ratio)) will improve the thixotropic behaviour of bentonite particles suspensions and dispersions [78]. It has been also found that CMC has the ability to suspend the clay particles in the polymer solution and delay their precipitation at the bottom of the electrospinning bath. This is due to the carboxyl group in the CMC which causes water dispersibility and an increase in the apparent and plastic viscosity [81]. Based on the advantages of CMC and Na_2CO_3, we have purified, activated and mixed the low cost bentonite clay with CMC and Na_2CO_3 rather than buying Sodium montmorillonite clay. In order to obtain a stable and uniform suspension of BC in the CA solution, 4 wt.% of CMC was added to the hot wet activated BC. By mixing Na_2CO_3 before adding the CMC, it is possible to promote an efficient reaction because the CMC hydrogel can obstruct the reaction in which the Ca^+ ions are exchanged by Na^+ ions [79]. Figure 1 summarises the stages forms of the BC obtained through processing, from the original mined state.
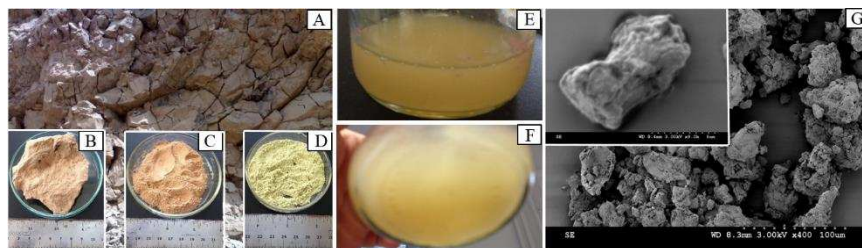
Figure 1. (A) Naturally occurring BC, (B) crushed BC, (C) ground BC, (D) sieved, purified and activated BC, (E, F) uniform solution of CA loaded with purified, activated and dispersed BC and (G) SEM images of raw untreated BC micro stones.

Electrospinning of CA/BC Composite Nanofibrous Fabrics

Figure 2 shows the electrospinning set up using the wire electrode. As the electrode rotates through the polymer solution, a thin film of charged liquid is formed on the wire. As the wires emerge from the polymer solution the film on the wire undergoes Plateau–Rayleigh instability resulting in multiple droplet formation along the length [69]. If the electric field is sufficiently high, jets of polymer solution form from the droplets to produce filaments that can be collected above, as shown in Figure 2.

Using wires or cylindrical electrodes, we have found that fibre formation is similar for both, but there are differences in the droplet formation mechanism, shape and size. With the wire electrode droplet formation depends on viscosity, surface tension and electrical conductivity of the polymer solution, the rotational speed and the applied electric field. Based on experience of the both systems, we suggest that it is desirable to operate the cylindrical electrode system with a low polymer solution concentration, and a lower viscosity than for the wire electrode. In the present experiments using the wire electrode, a spinning solution of 15 wt.% CA with (0 – 25 wt.%) BC loading was found to yield the highest productivity and electrospinning stability. The optimal voltage range was 65-75 kV using a 12 cm spinning distance. As the BC loading increased, so too did the viscosity and surface tension, requiring a higher voltage and lower wire rotation speed to maintain stable spinning conditions.
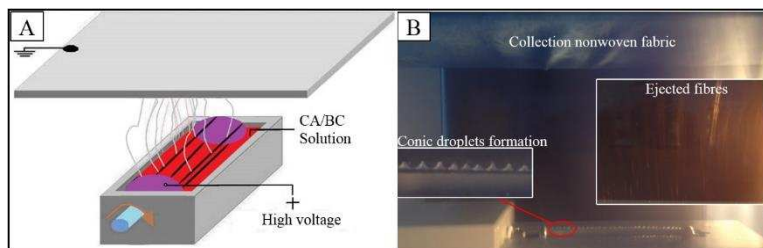
Figure 2. (A) schematic of the free surface electrospinning set-up based on a four wire spindle electrode, (B) real image of the free surface electrospinning set-up using a four wire spindle electrode and a nonwoven PP fabric collector. Inset is a magnified image of conical droplet formation.

Morphology of HCl Purified and Na_2CO_3 Activated BC and CA/BC Composite Nanofibres

SEM images of HCl purified and Na_2CO_3 activated BC are shown in Figure 3 and pronounced differences were noted in the respective architectures. The HCl purified BC particle sizes in Figure 3(A), ranged from c. 5 μm - 60 μm with evidence of aggregation, and porosity in the exposed BC surfaces. In Figure 3(B) the Na_2CO_3 activated and HCl purified BC and reacted with CMC and (AcOH: water) (75/25, v/v) as a mimicry to the BC state during electrospinning. There was a decrease in the size of BC particles and an increase in the apparent porosity of the BC surface compared to the HCl purified BC. Note also that in Figure 3(B), the shape of the BC can be characterised as a flake-like sheet arranged in a layered formation. This is an indication of particle distortion, fragmentation and exfoliation by the action of AcOH, water, CMC and Na_2CO_3. In fact, the observations obtained herein are in reasonable agreement with those in the literature for BC [82]. Figure 3(C), shows a SEM image of electrospun purified and activated BC fibres produced from an (AcOH: water) solution. Electrospun BC particles attached to the PP spunbond nonwoven fabric were fragmented into particles as small as 100 nm of various shapes. Amrani et al. stated the cause of the separation of layers due to the phenomenon of hydrophobia with the migration of

hydronium ions towards the surface and the transformation of their crystal lattice [77]. However, we believe that the applied electric field plays a part in the fragmenting and disintegrating the BC during electrospinning, which is reflected by substantial difference in the clay sizes before and after electrospinning.

Typical SEM and TEM images of the CA nanofibres fabricated from a 15 wt.% CA solution in (AcOH: water) with 10 wt.% BC/CA loading are shown in Figure 4(A, B). All of the nanofibres were randomly distributed to form a porous web of nanofibres penetrating semi spherical features resembling jellyfish. The TEM image confirms that the different sizes and shapes of BC were incorporated within these jellyfish-like features.
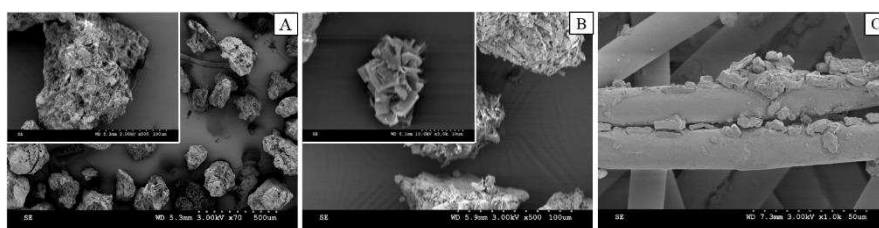

Figure 3. SEM images of (A) HCl purified BC, (B) Na_2CO_3 activated, HCl purified BC and reacted with CMC and (AcOH: water) and (C) electrospun purified and activated BC from (AcOH: water) solution.
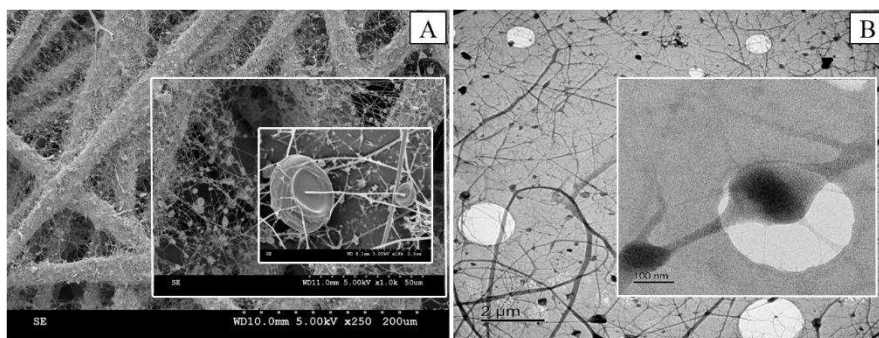

Figure 4. SEM (A) and TEM (B) images of CA nanofibres fabricated from a 15 wt.% CA solution with 10 wt.% BC/CA loading.

Figure 5 (A-I), presents SEM images of electrospun CA nanofibres in Figure 5(A), CA/BC composite nanofibres with different BC loadings in Figures 5(B-F) and (G) fibre diameter distributions of image (A) and (H, and I) diameter distributions of jellyfish features of image (B) and image (C), respectively. Fabric of CA nanofibres loaded with BC were readily electrospun forming fibres ranging from 30 to 280 nm with mean fibre diameters of 70-100 and positively skewed diameter distributions and the jellyfish features ranging from 100 nm to 2.5 µm in diameter with mean diameter of 0.5-0.7 µm and positively skewed diameter distributions. It is evident that, at higher BC loading, the formation of continuous composite nanofibres was difficult due to the inability to preserve stable flow of the polymer solution loaded with clay from the droplets on the wire electrode. Briefly, electrospun nanofibres loaded with activated BC with a smaller diameter and thus a higher surface area could be produced uniformly when the BC loading was reduced to 5 - 10 wt.%, but non uniform fibres and beads were formed if the loading was increased to 15 - 25 wt.%. Nevertheless, the electrospun nanofibre diameters resulting from 15 wt.% CA solutions were nearly the same at all BC/CA loading levels as shown in Figure 5.

The interior morphologies of CA/BC nanofibres for all samples were studied using TEM as shown in Figure 6(A-F). Figure 6(A), shows dark spots which correspond to the BC lamella inside the jellyfish features. The encapsulated BC within these features were of different sizes and shapes and were well distributed within the CA fabric when the BC loading was low, see Figure 6(B, C).

The BC preferentially resided within the interior and at the interfacial regions. By contrast, as shown in Figure 6(D-F) poor dispersion and interfacial contact of the BC occurred when the loading concentration increased to more than 15 wt.%. This is to be expected for two reasons. Firstly, the stress resulting from agglomeration of BC at high loadings and secondly, the high loading of BC is likely to increase the surface tension and viscosity of the polymer solution, leading to instability during the electrospinning process. As a result, we have found that the maximum BC loading to obtain optimal dispersion and distribution of BC within the CA

nanofibrous structure is 10 wt.%. While, if the loading increases to 15, 20 or 25 wt.% bead formation is prevalent.

The elemental analysis of HCl purified BC compositions were confirmed by the EDX analysis in Figure 7(A). Note that the HCl purified BC consisted mainly of O, Si, Fe, Al, and Mg as inorganic bases for the metal oxides SiO_2, Al_2O_3, Fe_2O_3 and MgO, which are instrumental in providing material functionality [2]. Figure 7(B), reflects the TEM and EDX data for CA15BC5 and the embedding of BC within the CA nanofibres. The EDX spectra recorded at specific points revealed C, O, Na, Mg, Al, Si, Ca and Fe in the CA, semi-spherical jellyfish-like features, penetrated by CA nanofibre. Note also that the existence of C, Na are indicative of CA with a Na_2CO_3 activated component.
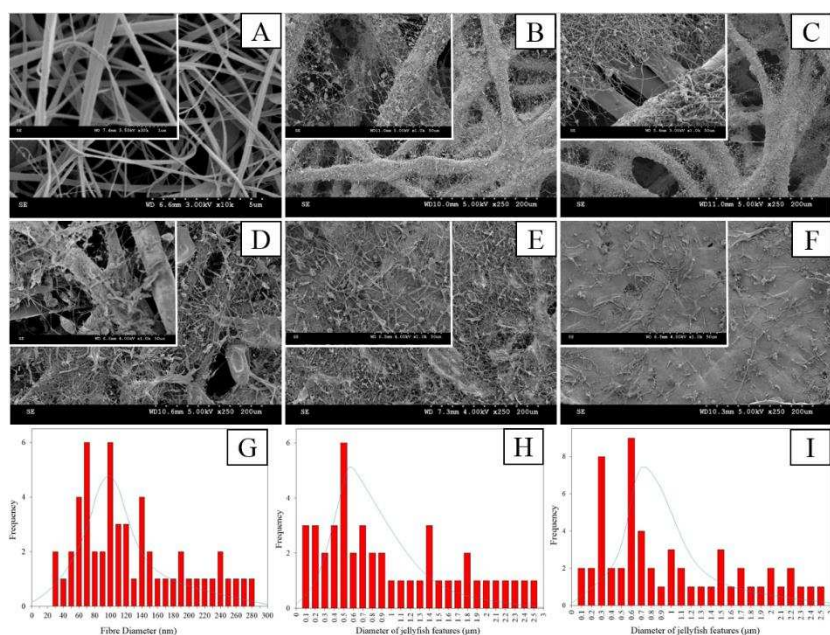

Figure 5. SEM images of CA and CA/BC nanofibres. (A) SEM image of electrospun CA nanofibre at 15wt.% CA solution. SEM images of CA15BC5 (B), CA15BC10 (C), CA15BC15 (D), CA15BC20 (E), and CA15BC25 (F).
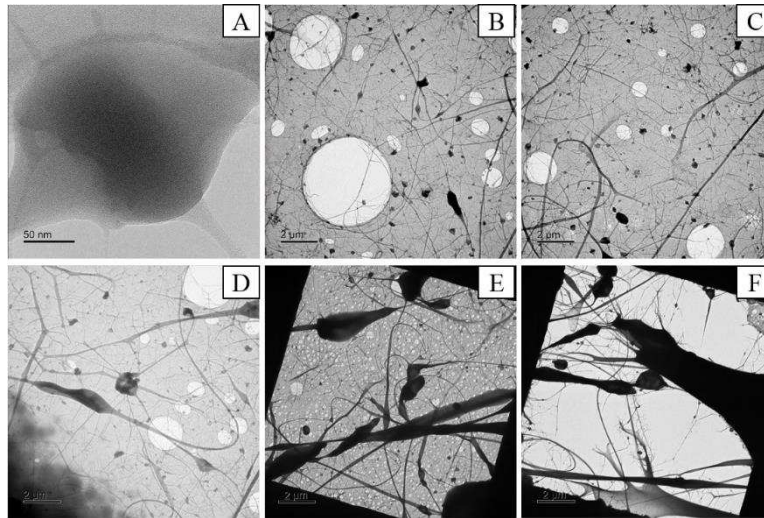
Figure 6. TEM images of electrospun CA/BC composite nanofibres. (A) TEM image of CA15BC10 at 50 nm bar. TEM images of CA15BC5 (B), CA15BC10 (C), CA15BC15 (D), CA15BC20 (E) and CA15BC25 (F).
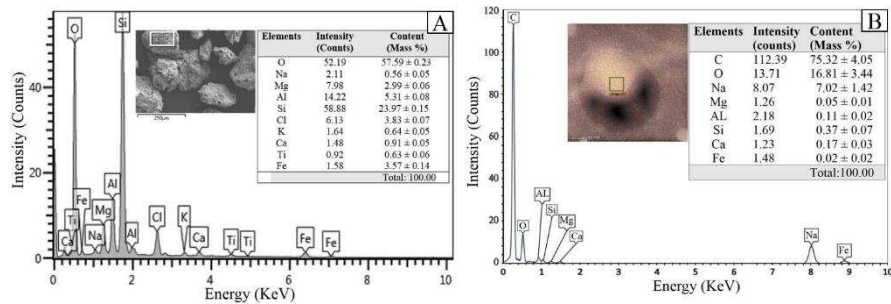
Figure 7. (A) SEM/EDX elemental analysis of HCl purified BC compositions. (B) TEM/EDX composition elemental analysis of 15 wt.% CA solution with 5 wt.% BC/CA loading rate.

A nanoscale TEM-EDX elemental quantitative mapping in Figure 8, detected C as a primary component of the CA/BC composite nanofibrous fabric, and the BC layers consisted of O, Al, Si, Fe, Na, Mg and Ca distributed in varying proportions throughout the CA nanofibrous fabric.

Viscosity, Surface Tension and Electrical Conductivity of CA/BC Solutions

Free surface electrospinning can only be accomplished when process parameters are conveniently controlled, such as evaporation rate of the solvent, as well as viscosity, surface tension and electrical conductivity of the electrospinning polymer solution. Convenient evaporation rates for CA/BC spinning are critical to ensure stable fibre production, since solvents having high evaporation rates such as acetone, chloroform and methanol, tend to obstruct jet formation from droplets on the electrode wires [83]. On the other hand, very low evaporation rates lead to film rather than fibre formation. By selecting a binary solvent system of AcOH and water (75:25) with boiling point of 118°C, 100 °C respectively, stable spinning conditions were achieved [84] and it is well established that when the ratio of AcOH to water is 75:25, nanofibrous cellulose fibres can be successfully generated without formation of beads [24].

The shear viscosities of dissolved CA at concentration of 15% (w/v) and CA/BC at various loading rate of BC are plotted in Figure 9(A). The shear viscosities of the CA/BC increased with increasing BC concentration which is to be expected. A higher shear viscosity was observed for CA15BC25 due mainly to the incorporation of a high clay loading rather than the molecular weight of the CA. In Figure 9(A), the CA/BC shear viscosity values at a 0.017 sec^{-1} shear rate, mimic the prevailing conditions due to the revolution of the wire electrode at 1 r min^{-1}. Indeed, these viscosity values necessitated the use of voltages of at least 65 kV for CA15BC0 and 75 KV for CA15BC25 to induce electrical forces high enough to overcome the viscoelastic forces needed to form jets from droplets on the electrode wires [65].

The surface tension of dissolved CA at a concentration of 15% (w/v) and CA/BC at various BC loadings are given in Figure 9(B). The surface tension values of the CA/BC decreased with a decrease in BC concentration. For example the surface tension decreased from 41.62±1.2 mN/m for CA15/BC25 to 34.85±0.5 mN.m^{-1} for CA15BC5 and to 32.35±0.45 mN.m^{-1} for CA15BC0. It has been observed that there is a

direct correlation between the uniformity of fibre diameter, polymer solution viscosity and surface tension [85]. The SEM image in Figure 5(D-F), clearly reveals the formation of beaded structures and the aggregation of BC as its concentration increased. SEM images clearly revealed that beaded nanofibres and agglomerated BC formed if the surface tension and viscosity were too high. It has been reported that the AcOH concentration in water strongly affects the surface tension, and it can be reduced by increasing the AcOH concentration in water [86].
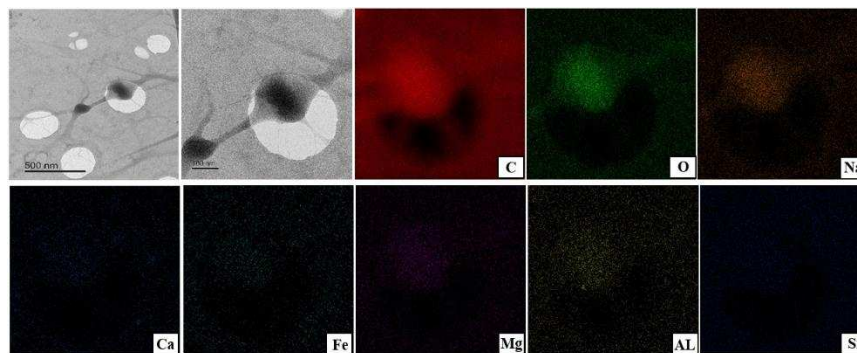

Figure 8. TEM images of 15 wt.% CA solution with 10 wt.% BC/CA loading and mapping images showing the existence of BC layers, composed of C, O, Na, Ca, Fe, Mg, AL and Si within the CA/BC composite nanofibres.
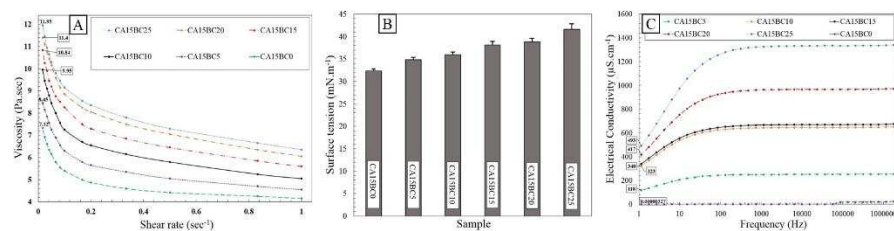

Figure 9. (A) Viscosity measurements as a function of shear rate, (B) averaged values of surface tension, (C) electrical conductivity measurements as a function of frequency for electrospun CA15BC0 nanofibres, CA15BC5, CA15BC10, CA15BC15, CA15BC20 and CA15BC25 composite nanofibres.

Electrical conductivity as a function of frequency is presented in Figure 9(C), for samples of dissolved CA at a concentration of 15% (w/v) and CA/BC at various BC loadings. The value of the electrical conductivity at the lowest measured nearly zero frequency has been considered as a direct current (DC) conductivity for comparative purpose which suits the case of the DC high voltage power supply used in our work. However, Figure 9(C), reveals that electrical conductivity increases as the frequency increases. Therefore, differences between all dissolved CA/BC solutions were assessed at the lowest frequency (1.0 Hz, nearly zero). For the dissolved CA/BC at various BC concentrations the electrical conductivity increased as the BC concentration increased. For example the electrical conductivity increases from 0.00000327 μS.cm^{-1} (nearly zero) for CA15BC0 to 118 μS.cm^{-1} for CA15BC5 and to 493 μS.cm^{-1} for CA15BC25. It is clear that with the increasing of BC concentration, the charge density of the CA/BC solution increased. As a matter of fact, the electrical conductivity of the polymer solution mirrors the charge density on the jet and thus the higher elongation forces that are imposed on the fibres during spinning subject to the applied electrical field, leading to smaller fibre diameters.

Structure and Thermal Properties of CA/BC Composite Nanofibrous Fabrics

Figure 10, shows the wide angle X-ray diffraction (WAXD) patterns of purified and activated BC, CA15BC0, CA15BC5 and CA15BC10 composite nanofibrous fabrics to indicate the distribution of BC layers in the CA/BC composites. The XRD pattern of purified and activated BC shows one intense diffraction peak around about $2\theta = 27.2°$ due to quartz which tends to form the highest peak. This peak indicates the distance between the adjacent BC lamellar structure, being approximately $2\theta = 27.2°$, d= 15.62 A° (1.562 nm) according to Bragg's law. The other low intensity peaks indicate that the BC is enriched with amorphous phases [82]. The XRD pattern of electrospun CA15BC0 nanofibres shows broad

weak diffraction peaks at approximately $2\theta = 9.4°$ and $2\theta = 44.8°$ which are associated with the principal characteristic of the semi-crystalline acetylated structure of cellulose acetate [87]. The absence of BC peaks from the XRD patterns of CA15BC5, CA15BC10 composites confirmed that most of the BC had been exfoliated, delaminated and dispersed in the CA nanofibrous fabric [24]. However, XRD pattern of CA15BC10 shows two diffraction peaks with low intensity at $2\theta = 47.8°$ and $2\theta = 46.8°$, which could be an indicator of partly stuffing of BC within the CA composites.

The thermal stability and behaviour of the purified and activated clay (BC) and electrospun CA/BC nanofibres were evaluated using TGA and DSC in a nitrogen atmosphere. Figure 11 shows the TGA thermograms of BC, CA15BC0 nanofibres and CA15BC5 and CA15BC10 composite nanofibres. As shown in Figure 11, the thermal stability of BC is high, hence only 17.67 wt.% of BC is decomposed at 600°C. The TGA curves of CA and CA/BC fabrics manifest three phases of degradation which are different in comparison with pure BC which has nearly linear degradation rate. Table 3 shows the values of the yield of charred residue wt.% at 600°C and decomposition temperature at the onset and at 20% degradation rate of pure BC and CA15BC0, CA15BC5 and CA15BC10 fabrics. Generally, the initial weight loss from 40 °C to 120°C is considered due to the evaporation of the absorbed water and the organic solvent (AcOH) trapped in the composite nanofibres and between the clay layers [14]. The onset degradation (nearly 4 wt.% weight loss) of CA/BC fabrics reduced from 240°C for the CA15BC0 nanofibres to 230°C for the CA15BC5 nanofibres and 220°C for the CA15BC10 nanofibres. In addition, the decomposition temperatures at 20% degradation rate were 272°C for the CA15BC0 nanofibres and 249°C and 237°C for CA15BC5 and CA15BC10, respectively. These reductions in the onset degradation and at 20% degradation rate temperatures were explained that the alkylammonium cations of clay were thermally unstable and decomposed at lower temperatures [24]. It is worth noting that the adsorption of alkylammonium cations from aqueous solution by montmorillonite has been occurred through an exchange reaction between the inorganic cations

on the clay and the alkylammonium ions in the aqueous (AcOH (75:25, v/v)) solution [88]. In the second phase, significant weight loss was observed due to thermal degradation. For CA15BC0 nanofibres, nearly 75% of the sample degraded from 245 to 350°C. This wide temperature range to the molten phase is due to the large amorphous region. After polymer dissolution and electrospinning, the internal structure of the electrospun and native materials differs. The area of the amorphous region increases and the total crystallisation area decreases [89]. On the other hand, from the yield of charred residue data at 600°C, an improvement in the thermal stability can be proved when BC loading is increased. For instance, the yield of charred residue after thermal decomposition at 600°C is increased from 11.96 wt.% for the CA15BC0 nanofibres, to 15.12 wt.% for the CA15BC5 nanofibres and 18.06 wt.% for the CA15BC10 nanofibres. In other words, the TGA curves distinctly indicate that the thermal stability of CA nanofibres is enhanced by increasing the loading of the BC which acts as a superior insulator and mass transport barrier resulting in oxygen and heat permeability reductions in the CA/BC matrix during the heating exposure [14, 24, 90].
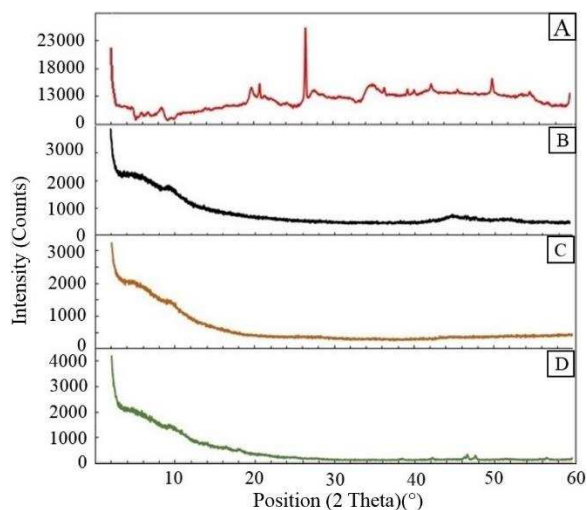

Figure 10. WAXD of BC (A) and CA15BC0 (B), CA15BC5 (C) and CA15BC10 (D) composite nanofibres.
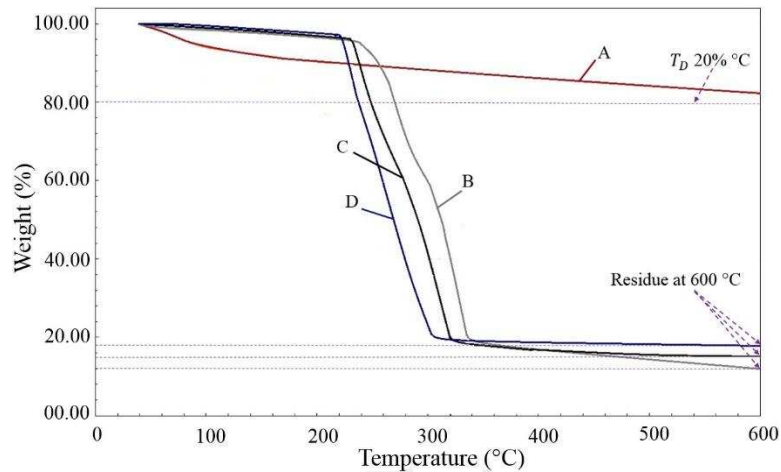
Figure 11. TGA thermograms of purified and activated BC (A), CA15BC0 nanofibres (B) and CA15BC5 (C) and CA15BC10 (D) composite nanofibres.

Table 3. The residue % at 600°C and decomposition temperature at the onset and at 20% degradation rate of purified and activated BC and CA/BC electrospun nanofibres (CA15BC0, CA15BC5 and CA15BC10)

Materials	T_D Onset (°C)	T_D 20% (°C)	Residue at 600 °C (%)
Purified and activated BC	----------	----------	82.33
CA15BC0	240	272	11.96
CA15BC5	230	249	15.12
CA15BC10	220	237	18.06

Figure 12, shows the DSC curves of BC and CA/BC composite nanofibrous fabrics. It can be found from Figure 12(A), that the DSC curve of BC showed one endothermic heat peak at 91.35°C due to loss of adsorbed water [91]. Figure 12(B), presents the DSC thermogram of CA which shows an endothermic heat peak located at 83.84°C due to outflow and evaporation of the absorbed water [92]. In addition, an endothermic heat peak occurred at 362.48°C which is attributed to the melting of the semi-crystalline regions and degradation of CA material. The endotherm of fusion for electrospun cellulose acetate nanofibres located at approximately

360°C indicates their semi-crystalline character shown by the WAXD diffraction patterns which refer to the contributions of the amorphous and semi crystalline regions. These results are in agreement with the published work of thermal properties of electrospun cellulose acetate nanofibres by Zahedi et al. [93]. It is also observed that the melting peak temperature of CA15BC5 is around 378.88°C and the melting peak temperature of CA15BC10 is at 401.18°C, which both are slightly higher than that of the neat CA electrospun nanofibres. It was also observed that higher values of enthalpy of crystallisation and fusion were found for CA15BC5 and CA15BC10 samples as shown in Figure 12(C, D). Therefore, this indicates that the BC layers are existent in CA/BC nanofibres and also make these composite nanofibres more thermally stable.
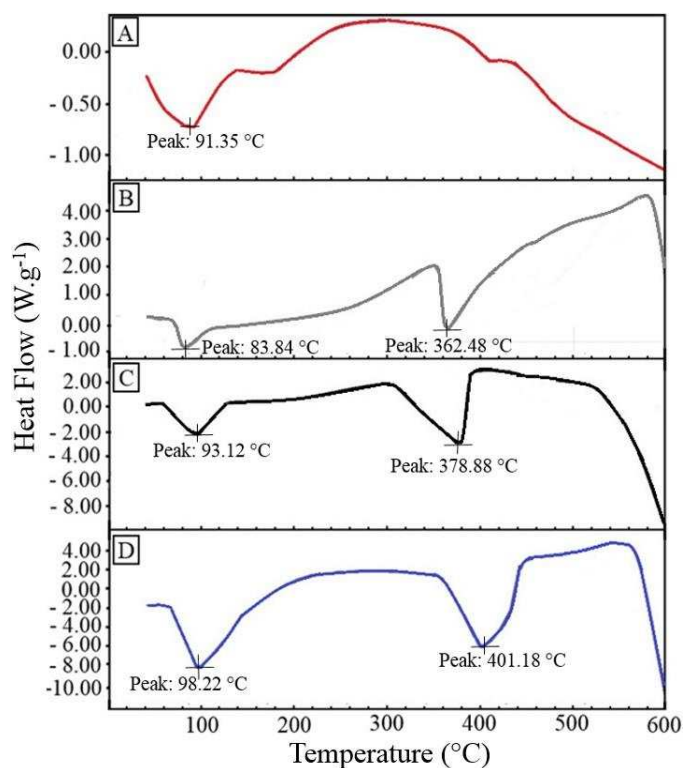

Figure 12. DSC thermograms of purified and activated BC (A), CA15BC0 nanofibres (B) and CA15BC5 (C) and CA15BC10 (D) composite nanofibres.

FUTURE PERSPECTIVES

The use of adsorbents such as activated bentonite clay and activated carbon in environment and industry is an established strategy for adsorption of inorganic and organic pollutants. In this regard, four key questions can be addressed and answered:

What Is the Problem with the Existing Adsorption Process?

The main problems of the existing processes based on adsorption can be summarised by reviewing them from two angles.

In case of which the adsorbents are applied in the powder or granular form, there are some issues, which restrict the practical applications of these macro, meso, micro and nano-structured adsorbents and might affect their performance. First, due to the high surface energy of adsorbents, their tendency to grow and form hard agglomerates is quite strong, reducing thereby the surface area and the accessible active sites available for adsorption reactions, and second, the additional separation process of adsorbents from the reaction solution either by filtration or by centrifugation is quite nontrivial on large scales [94]. Briefly, this creates challenges during their use in terms of handling and reusability.

In case of which the conventional porous (polymeric-ceramic) membranes are applied as adsorbents, they suffer from a serious loss of flux when pore sizes are reduced to improve their selectivity [95]. Moreover, the formation of biofilm on the membrane surface and clogging of the membrane pores are two major factors in membrane fouling due to their hydrophobic nature, geometrical structure of pores, the corresponding pore size distribution, undesirable macro-void formation across the whole membrane thickness and the lack of antimicrobial activity, which can reduce separation performance of the membranes and shorten membrane lifetime [96]. In addition, membranes fabricated by the conventional approach often suffer from the formation of pinholes and cracks during the

drying and calcination processes. These problems cause a high rate of defects and thus inflate the costs of the products [97].

What Is the Need?

To solve these problems in the existing adsorption process (adsorbents powder and membranes), a radical change is necessary, particularly in the texture of the separation layer that controls the performance of the resultant membrane in terms of flux and selectivity. In general, separation and adsorption performance, permeability and lifetime of the membranes mainly depend on porous structure and porosity of the membranes and membrane resistance to fouling since (1) membranes with larger surface to mass ratio, lower density and pore sizes, and higher porosity exhibit higher separation efficiency, (2) membranes with antifouling property indicate higher separation performance and longer lifetime [98]. It is well-known that a nanofibrous structure formed from nanofibres represents the most efficient structure for pressure-driven membrane-selection processes [12]. Such structures are able to achieve high selectivity while maintaining a high flux because the nanofibres divide large voids into smaller ones without forming dead-end pores and with a minimum reduction of the total void volume [99]. The porosity in the separation layer of nanofibres can be over 70% of its volume [2]. In contrast, the separation layer in conventional membranes has a porosity of below 36% and inevitably includes dead-end pores that make no contribution to the flux [2]. Moreover, the smaller the fibre diameter, the greater the surface area for particle adsorption and the better the retention of small particles [100]. Therefore, polymer–inorganic composite nanofibrous membrane, where inorganic adsorbents such as bentonite clay and activated carbon are incorporated and supported into the polymer nanofibres to prevent their coalescence is insistent. By having the ability to mass-produce nanofibres and to create multi-channelled reaction spaces convenient for mass transfer, and remarkably increase the accessible surface areas for removing of pollutants with higher efficiency, a great technical approach will be

achieved. The growing demand of high performance and low cost devices for effective adsorption leads to the greater attention toward the advanced nanoscale materials for micro and nano filtration, substances adsorption, gas separation and diffusion dialysis, etc. and to prevent harmful adsorbents from getting into the environment and the human body.

Why Should the Current Users Change to a Different Process?

In principle, using nanofibrous membrane with accessible routs towards the incorporated adsorbents to construct the separation layer is an effective approach for developing efficient separation membranes. This technical approach has significant advantages over reverse osmosis membranes include low operating pressure, high permeate flux and high rejection of low molecular weight organic compounds such as divalent salts and dyes. Moreover, they offer four goals (1) the potential of novel applications through the addition of optical, biological, electrical, antimicrobial via silver ions incorporation, and/or magnetic functionality, (2) the substantial increase in surface area to mass ratio of the nanofibrous membrane compared to that of bulk material would increase their adsorption capacities very significantly, (3) they are low-cost, easy operating conditions, high metal binding capacities, its high removal efficiency without the production of harmful by-products and (4) they can be utilised for in situ treatment of the contaminated medium as compared to the ex situ due to their small size, which further improves the economy of the medium treatment process.

How Viable Is It to Use the New Nanofibrous Membrane in the Particular Application?

The above indicated highly porous adsorptive nanofibrous membrane could be very promising where effective adsorption process is required by taking the advantage of the almost null pressure drop caused by these

structures and in underpinning development of novel tools and techniques. This technical approach has the potential in future to develop the next generation of effective membranes and to revolutionise the current water filtration technology by providing cheaper and portable units consuming less energy. The nanofibrous membrane structure formed from nanofibres with multi-channelled reaction spaces into adsorbents is the most efficient structure for separation and adsorption processes because nanofibres are able to divide large voids into smaller ones without forming dead-end pores and with the minimum reduction of the available void volume. The porosity in the separation layer of nanofibres is much larger than that of the separation layer in conventional membranes. The fabrication of these membranes is relatively straightforward and economical, compared to that of conventional membranes, and this approach can be scaled up readily to fabricate nanofibrous membranes loaded with adsorbents for practical applications.

OUTLOOKS

Nanofibrous membranes incorporating accessible adsorbents is believed to be an efficient structure for pressure-driven membrane-selection processes. Nanofibrous membranes have significant advantages over reverse osmosis membranes, including low operating pressure and high permeate flux [2]. The gradual degradation of CA nanofiber surfaces via UV degradation for instance, as shown in Figure 13, is likely to create diffusion channels that can be expected to promote adsorption of organic pollutants and heavy metals ions with higher mass transfer and efficiency. The electrospun composite nanofibres will be exposed to UV irradiation to reduce the Ag^+ nanoparticles from silver nitrate and to ensure the photocatalytic degradation of the cellulose acetate and then will be applied as a single stage water resilience filter. In addition, it has been reported that incorporating semiconductor-mediated photocatalytic materials such as TiO_2 followed by UV irradiation will promote the photocatalytic degradation of the carrier nanofibres and the antifouling performance of

the nanofiltration membrane [2]. In addition, Cellulose acetate/Ag$^+$ will separate and attract microorganisms and selected metal ions from water. This is an area for further study.
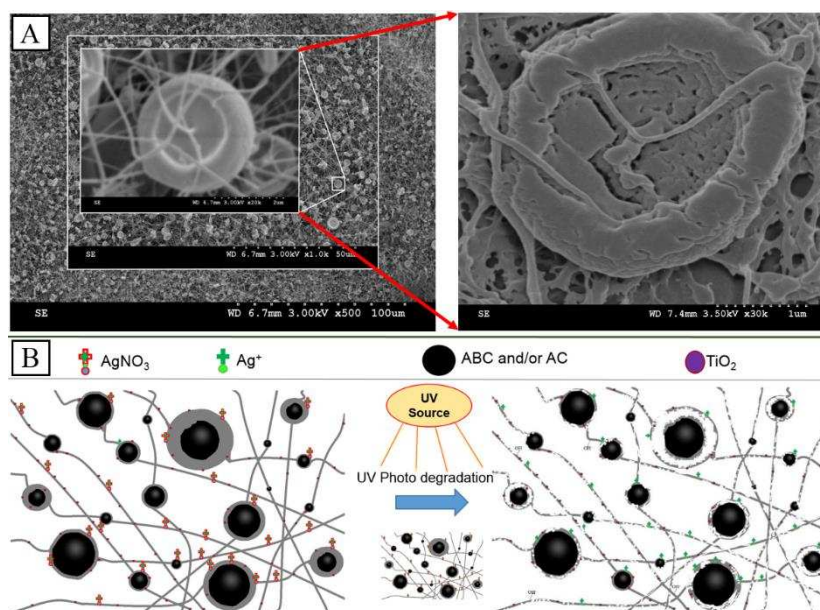

Figure 13. (A) SEM images of CA/BC nanofibres showing the stuffing of BC within the CA Jellyfish features nanofibres and how diffusion channels in the CA Jellyfish features nanofibres are created by degradation, (B) Schematic illustrations for the ABC and/or AC/AgNO$_3$/TiO$_2$ e incorporated electrospun cellulose acetate nanofibrous membrane by using Nanospider® based on free surface electrospinning. These electrospun composite nanofibres will be exposed to UV irradiation to reduce the Ag$^+$ nanoparticles from silver nitrate and to ensure the photocatalytic degradation of the cellulose acetate and then will be applied as a single stage water resilience filter.

CONCLUSION

A comprehensive review of electrospun nanofibres containing MMT as fillers and their proposed applications highlighted a significant focus on materials containing synthesised rather than naturally occurring MMTs. Herein, natural BC was investigated as a loading component in the manufacture of CA nanofibre webs. The natural BC was dried, crushed,

ground and sieved prior to before being purified with HCl and activated with Na_2CO_3. CMC was used to aid dispersion and suspension of BC prior to the production of BC-loaded CA nanofibre webs using free surface electrospinning. Optimal Nanospider electrospinning parameters for CA/BC were 65-75 kV and 12 cm for applied voltage and electrospinning working distance respectively. SEM images showed that all nanofibres were randomly distributed and inter-penetrated jellyfish-like semi-spherical features containing BC particles when the BC loadings were of 5, 10 wt.%. TEM confirmed that BC particles of different sizes and shapes were contained within these spatially distributed jellyfish-like features. When the BC loading increased to more than 15 wt.%, nonuniform/beaded CA/BC fabrics were formed. Electrospinning appears to play a role in reducing the particle size of natural BC due to the electrostatic forces, which means that pre-refining of natural BC to the final required particle size prior to free surface electrospinning is not necessary. In this work it has been demonstrated that up to 10wt% natural BC can be incorporated in CA nanofibre webs using an electrospinning process that is already available at industrial scale. Results from this study may provide the opportunity to transfer the composite nanofibres from experimental work to industrial production. In addition, we believed that this study may produce a novel engineered fabric material for human health, spas, aesthetic medicine and environmental applications such as rapid removal of organic micropollutants from liquids.

ACKNOWLEDGMENTS

REFERENCES

[1]   Bazbouz, M. B. & Stylios G. K. (2008). Alignment and optimisation of nylon 6 nanofibres by electrospinning. Journal of Applied Polymer Science, 107(5), 3023-3032.

[2]   Malwal, D. & Gopinath, P. (2016). Fabrication and applications of ceramic nanofibres in water remediation: A review. Critical Review Environment Science & Technology, 46(5), 500-534.

[3]   Sattar R., Kausar, A. & Siddiq, M. (2015). Advances in thermoplastic polyurethane composites reinforced with carbon nanotubes and nanofibres: A review. Journal of Plastic Film & Sheeting, 31(2), 186-224.

[4]   Hu, J., Kai, D., Ye, H., Tian, L., Ding, X. & Ramakrishna, S. (2017). Electrospinning of poly (glycerol sebacate) based nanofibres for nerve tissue engineering. Materials Science & Engineering C, 70, 1089-1094.

[5]   Li, D. & Xia, Y. (2004). Electrospinning of nanofibres: reinventing the wheel. Advanced Materials, 16, 1151-1170.

[6]   Su, Z., Ding, J. & Wei, G. (2014). Electrospinning: a facile technique for fabricating polymeric nanofibres doped with CNT and metallic nanoparticles for sensor applications. RSC Advances, 4, 52598-52610.

[7]   Bazbouz, M. B. & Stylios, G. K. (2010). The tensile properties of electrospun nylon 6 single nanofibres. Journal of Polymer Science (B) Polymer Physics, 48(15), 1719-1731.

[8]   Fong, H., Liu, W., Wang, C. S. & Vai, R. A. (2002). Generation of electrospun fibres of nylon 6 and nylon 6-montmorillonite nanocomposite. Polymer, 43(3), 775-780.

[9]   Li, L., Bellan, L. M., Craighead, H. G. & Frey, M. W. (2006). Formation and properties of nylon-6 and nylon-6/ montmorillonite composite nanofibres. Polymer, 47, 6208-6217.

[10]   Li, Q., Wei, Q., Wu, N., Cai, Y. & Gao, W. (2008). Structural characterisation and dynamic water adsorption of electrospun

polyamide6/montmorillonite nanofibres. Journal of Applied Polymer Science, 107, 3535-3540.

[11] Cai, Y., Huang, F., Wei, Q., Wu, E. & Gao, W. (2008). Surface functionalisation morphology and thermal properties of polyamide6/O-MMT composite nanofibres by Fe_2O_3 sputter coating. Applied Surface Science, 254, 5501-5505.

[12] Cai, Y., Huang, F., Wei, Q., Song, L., Hu, Y., Ye, Y., Xu, Y. & Gao, W. (2008). Structure, morphology, thermal stability and carbonisation mechanism studies of electrospun PA6/Fe-OMT nanocomposite fibres. Polymer Degradation & Stability, 93, 2180-2185.

[13] Cai, Y., Li, Q., Wei, Q., Wu, Y., Song, L. & Hu, Y. (2008). Structures, thermal stability, and crystalline properties of polyamide6/organic-modified Fe-montmorillonite composite nanofibres by electrospinning. Journal of Materials Science, 43, 6132-6138.

[14] Li, Q., Gao, D., Wei, Q., Ge, M., Liu, W., Wang, L. & Hu, K. (2010). Thermal Stability and Crystalline of Electrospun Polyamide 6/Organo-Montmorillonite Nanofibres. Journal of Applied Polymer Science, 117, 1572-1577.

[15] Cai, Y., Wu, N., Wei, Q., Xu, Q., Gao, W., Song, L. & Hu, Y. (2008). Structure, surface morphology, thermal and flammability characterisations of polyamide 6/organic-modified Fe-montmorillonite nanocomposite fibres functionalised by sputter coating of silicon. Surface and Coatings Technology, 203, 264-270.

[16] Agarwal A., Raheja, A., Natarajan, T. S., & Chandra, T. S. (2014). Effect of electrospun montmorillonite-nylon 6 nanofibrous membrane coated packaging on potato chips and bread. Innovative Food Science & Emerging Technologies, 26, 424-430.

[17] Wu, H., Krifa, M., Koo, J. H. (2014). Flame retardant polyamide 6/nanoclay/intumescent nanocomposite fibres through electrospinning. Textile Research Journal, 84(10), 1106-1118.

[18] Beatrice, C. A. G., Santos, C. R. D., Branciforti, M. C. & Bretas, R. E. S. (2012). Nanocomposites of polyamide 6/residual monomer with

organic-modified montmorillonite and their nanofibres produced by electrospinning. Materials Research, 15(4), 611-621.

[19] Yu, T., Lin, J., Xu, J., Chen, T. & Lin, S. (2005). Novel polyacrylonitrile nanocomposites containing Na-montmorillonite and nano SiO$_2$ particle. Polymer, 46, 5695-5697.

[20] Qiao, H., Cai, Y., Chen, F., Wei, Q., Weng, F., Huang, F., Song, L., Hu, Y., Gao, W. (2009). Influences of organic-modified Fe-montmorillonite on structure, morphology and properties of polyacrylonitrile nanocomposite fibres. Fibres & Polymers, 10(6), 750-755.

[21] Shami, Z., Sanjani, N. S. (2010). The role of Na-montmorillonite on thermal characteristics and morphology of electrospun PAN nanofibres. Fibres & Polymers, 11(5), 695-699.

[22] Wang, Q., Li, G., Zhang, J., Huang, F., Lu, K. & Wei, Q. (2014), PAN nanofibres reinforced with MMT/GO hybrid nanofillers, Journal of Nanomaterials, 2015, 298021, 10.

[23] Almuhamed, S., Bonne, M., Khenoussi, N., Brendle, J., Schacher, L., Lebeau, B. & Adolphe, D. C. (2016). Electrospinning composite nanofibres of polyacrylonitrile/synthetic Na-montmorillonite. Journal of Industrial and Engineering Chemistry, 35, 146-152.

[24] Kim, S. W., Han, S. O., Sim, N., Cheon, J. Y. & Park, W. H. (2015). Fabrication and characterisation of cellulose acetate/montmorillonite composite nanofibres by electrospinning. Journal of Nanomaterials, 2015, 275230, 8.

[25] Mingyu, J. Z., Wang, S. X., Wu, J., Yang, Z., Cao, J., Chen, Y. & Wei, Q. (2016). Preparation of a cellulose acetate/organic montmorillonite composite porous ultrafine fibre membrane for enzyme immobilisation. Journal of Applied Polymer Science, 133(33), 43818-43825.

[26] Kalaoglu, O., Unlu, C. H., Atici & O. G. (2016). Synthesis, characterisation and electrospinning of corn cellulose-graft-polyacrylonitrile and their clay nanocomposites. Carbohydrate Polymers, 147, 37-44.

[27] Cai, J., Lei, M., Zhang, Q., He, J. R., Chen, T., Liu, S., Fu, S. H., Li, T. T., Fei, P. (2017). Electrospun composite nanofibre mats of cellulose @ organically modified montmorillonite for heavy metal ion removal: design, characterisation, evaluation of absorption performance. Composites (A), 92, 10-16.

[28] Lee, H. W., Karim, M. R., Ji, H. M., Choi, J. H., Gim, H. D., Park, S. M., Weontae, O. & Yeum, J. H. (2009). Electrospinning fabrication and characterisation of poly (vinyl alcohol)/montmorillonite nanofibre mats. Journal of Applied Polymer Science, 113, 1860-1867.

[29] Ji, H. M., Lee, H. W., Karim, M. R., Cheong, I. W., Bae, E. A., Kim, T. H., Islam, M. S., Ji, B. C. & Yeum, H. (2009). Electrospinning and characterisation of medium molecular weight Poly(vinyl alcohol)/high-molecular-weight poly (vinyl alcohol)/montmorillonite nanofibres. Colloid and Polymer Science, 287, 751-758.

[30] Park, J. H., Karim, M. R., Kim, I. K., Cheong, I. W., Kim, J. W., Bae, D. G., Cho, J. W., Yeum, J. H. (2010). Electrospinning fabrication and characterisation of poly (vinyl alcohol) /montmorillonite/silver hybrid nanofibres for antibacterial applications. Colloid and Polymer Science, 288, 115-121.

[31] Liu, Y. L., Li, Y., Xu, J. T. & Fan, Z. Q. (2010). Cooperative effect of electrospinning and nanoclay on formation of polar crystalline phases in poly (vinylidene fluoride). ACS Applied Materials and Interfaces, 2, 1759-1768.

[32] Lopes, A. C., Ferreira, J. C. C., Costa, C. M. & Mendez, S. L. (2013). Crystallisation kinetics of montmorillonite /poly (vinylidene fluoride) composites and its correlation with the crystalline polymer phase formation. Thermochimica Acta, 574, 19-25.

[33] Fang, C., Yang, S., Zhao, X., Du, P. & Xiong, J. (2016). Electrospun montmorillonite modified poly (vinylidene fluoride) nanocomposite separators for lithium-ion batteries. Materials Research Bulletin 79, 1-7.

[34] Hong, J. H., Jeong, E. H., Lee, H. S., Baik, D. H., Seo, S. W & Youk, J. H. (2005). Electrospinning of polyurethane/ organically modified

montmorillonite nanocomposites. Journal of Polymer Science B: Polymer Physics, 43, 3171-3177.

[35] Saha, K., Butola, B. S. & Joshi, M. (2014). Drug-Loaded polyurethane/clay nanocomposite nanofibres for topical drug-delivery application. Journal of Applied Polymer Science, 131(10), 40230-40238.

[36] Ortenzi, M. A., Basilissi, L., Farina, H., Silvestro, G. D., Piergiovanni, L., Mascheroni, E. (2015). Evaluation of crystallinity and gas barrier properties of films obtained from PLA nanocomposites synthesised via ''in situ'' polymerisation of L-lactide with silane-modified nanosilica and montmorillonite. Eur Polym J, 66, 478-491.

[37] Lee, Y. H., Lee, J. H., An, I. G., Kim, C., Lee, D. S., Lee, Y. K., Nam, J. D. (2005). Electrospun dual-porosity structure and biodegradation morphology of Montmorillonite reinforced PLLA nanocomposite scaffolds. Biomaterials, 26, 3165-3172.

[38] Kishimoto, Y., Ito, F., Usami, H., Togawa, E., Tsukada, M., Morikawa, H., Yamanaka, S. (2013). Nanocomposite of silk fibroin nanofibre and montmorillonite: fabrication and morphology. Int J Biological Macromole, 57, 124-128.

[39] Chen, X., Gao, H., Ploehn, H. J. (2014). Montmorillonite- levan nanocomposites with improved thermal and mechanical properties. Carbohydr Polym, 101, 565-573.

[40] Ayutthaya, S. I. N., Tanpichai, S., Sangkhun, W., Wootthikanokkhan, J. (2016). Effect of clay content on morphology and processability of electrospun keratin/poly (lactic acid) nanofibre. Int J Biological Macromole, 85, 585-595.

[41] Islam, M. S., Yeum, J. H., Das, A. K. (2012). Effect of pullulan/poly (vinyl alcohol) blend system on the montmorillonite structure with property characterisation of electrospun pullulan/poly(vinyl alcohol)/montmorillonite nanofibres. J Colloid & Interface Sci, 368, 273-281.

[42] Islam, M. S., Rahaman, M. S., Yeum, J. H. (2015). Electrospun novel super-absorbent based on polysaccharide-polyvinyl alcohol-montmorillonite clay nanocomposites. Carbohydr Polym, 115, 69-77.

[43] Ma, Y., Li, L. B., Gao, G. X., Yang, X. Y., You, Y. (2016). Effect of montmorillonite on the ionic conductivity and electrochemical properties of a composite solid polymer electrolyte based on polyvinylidenedifluoride/ polyvinyl alcohol matrix for lithium ion batteries. Electrochimica Acta, 187, 535-542.

[44] Park, J. H., Lee, H. W., Chae, D. K., Oh, W., Yun, J. D., Deng, Y., Yeum, J. H. (2009). Electrospinning and characterisation of poly (vinyl alcohol)/chitosan oligosaccharide/clay nanocomposite nanofibres in aqueous solutions. Colloid & Polym Sci, 287, 943-950.

[45] Bunyatova1, U., Rzayev, Z. M. O., Şimşek, M. (2016). Multifunctional e-spun colloidal nanofibre structures from various dispersed blends of PVA/ODA-MMT with PVP/ODA-MMT, poly (VP-alt-MA) and AgNPs incorporated polymer complexes as electro-active platforms. EXPRESS Polym Lett, 10(7), 598-616.

[46] Simsek, M., Rzayev, Z. M. O., Acar, S., Salamov, B., Bunyatova, U. (2016). Novel colloidal nanofibre electrolytes from PVA-organoclay/ poly (MA-ALT-MVE), and their NaOH and ag-carrying polymer complexes. Polym Eng & Sci, 56(2), 204-213.

[47] Simsek, M., Rzayev, Z. M. O., Bunyatova, U. (2016). Multifunctional electroactive electrospun nanofibre structures from water solution blends of PVA/ODA–MMT and poly (Maleic acid-ALT-Acrylic acid): effects of Ag, organoclay, structural rearrangement and NaOH doping factors. Adv Natural Sci: Nanosci & Nano-technol, 7(2), 025009-0250013.

[48] Rzayev, Z. M. O., Simsek, M., Bunyatova, U., Salamov, B. (2016). Novel colloidal nanofibre semiconductor electrolytes from solution blends of PVA/ODA–MMT, poly (itaconicanhydride-alt-2-vinyl-1, 3-dioxalan) and its Ag-carrying polymer complex by reactive electrospinning. Colloids & Surfaces A: Physicochem Eng Aspects, 492, 26-37.

[49] Wang, M., Hsieh, A. J., Rutledge, G. C. (2005). Electrospinning of poly (MMA-co-MAA) copolymers and their layered silicate nanocomposites for improved thermal properties. Polymer 46, 3407-3418.

[50] Rzayev, M. O., Simsek, M., Salimi, K. (2015). Functional copolymer/organo-MMT Nanoarchitectures: fabrication and characterisation of electrospun nanofibres from PCL/ODA-MMT and copolymer-g-PLA/Ag-MMT blends. Polym-Plast Technol & Eng, 54, 1723-1734.

[51] Rzayev, Z. M. O., Erdonmez, D., Erkan, K., Bunyatova, M. U. (2015). Functional copolymer/organo-MMT nano-architectures. XXII. Fabrication and characterisation of antifungal and antibacterial poly (Vinyl Alcohol-co-Vinyl Acetate/ODA-MMT/AgNPs nanofibres and coatings by e-spinning and c-spinning methods. Int J Polym Mater & Polym Biomater, 64, 267-278.

[52] Kalgaonkar, R. A., Jog, J. P. (2007). Polyolefin/Clay Nanocomposites. In: Brown P. J., Stevens, K., editors. Nanofibres and Nanotechnology in Textiles. Cambridge: Woodhead publishing Ltd; 2007; pp 351-385.

[53] Haydel, S. E., Remenih, C. M., Williams, L. B. (2008). Broad-spectrum in vitro antibacterial activities of clay minerals against antibiotic-susceptible and antibiotic-resistant bacterial pathogens. J Antimicrobial Chemotherapy, 61, 353-361.

[54] Marini, M., Bondi, M., Iseppi, R., Toselli, M., Pilati, F. (2007). Preparation and antibacterial activity of hybrid materials containing quaternary ammonium salts via sol-gel process. Euro Polym J, 43, 3621-3628.

[55] Williams, L. B., Haydel, S. E. (2010). Evaluation of the medicinal use of clay minerals as antibacterial agents. Int Geology Rev, 52(7/8), 745-770.

[56] Carretero, M. I. (2002). Clay minerals and their beneficial effects upon human health. A review. Appl Clay Sci, 21, 155-163.

[57] Carretero, M. I., Lagaly, G. (2007). Clays and health: an introduction. Appl Clay Sci, 36, 1-3.

[58] Gomes, C. F., Silva, J. P. (2007). Minerals and clay minerals in medical geology. Appl Clay Sci, 3, 64-21.

[59] Al-Jlil, S. (2010). Removal of heavy metals from industrial wastewater by adsorption using local bentonite clay and roasted date pits in Saudi Arabia. Trends in Appl Sci Res, 5, 138-145.

[60] Zohra1, M., Rose, J., Borschneck, D. (2014). Urban wastewater treatment by adsorption of organic matters on modified bentonite by Iron-Aluminum. J Encapsul & Adsorp Sci, 4, 71-79.

[61] Bleifuss, R. L. (1973). Activation of non-swelling bentonite. Clay Minerals, 10, 41-55.

[62] Alther, G. R. (1982). The role of bentonite in soil sealing applications. Bulletin Assoc Eng Geology, 19(4), 401-409.

[63] Dosunmu, O. O., Chase, G. G., Kataphinan, W., Reneker, D. H. (2006). Electrospinning of polymer nanofibres from multiple jets on a porous tubular surface. Nanotechnology, 17, 1123-1127.

[64] Reneker, H., Yarin, A. L., Fong, H., Koombhongse, S. (2000). Bending instability of electrically charged liquid jets of polymer solutions in electrospinning. J Appl Phys, 87, 4531-4547.

[65] Bazbouz, M. B. (2009). An investigation of yarn spinning from electrospun nanofibres, PhD Thesis, Heriot Watt University, United Kingdom, URI: http://hdl.handle.net/10399/2245.

[66] Formhals, A. (1944). Method and apparatus for spinning. US Patent, 2349950.

[67] Jirsak, O., Sanetrnik, F., Lukas, D., Kotek, V., Martinova, L., Chaloupek, J. (2005). A method of nanofibres production from a polymer solution using electrostatic spinning and a device for carrying out the method. World Intellectual Property Organization Patent, WO024101.

[68] The Elmarco company (2018) http://elmarco.com. Accessed 09 January 2018.

[69] Forward, K. M., Rutledge, G. C. (2012). Free surface electrospinning from a wire electrode. Chem Eng J 183(15), 492-950.

[70] Park, H. M., Liang, X., Mohanty, A. K., Misra, M., Drzal, L. T. (2004). Effect of compatibilizer on nanostructure of the

biodegradable cellulose acetate/clay nanocomposites. Macromolecules, 37(24), 9076-9082.

[71] Konwarh, R., Karak, N., Misra, M. (2013). Electrospun cellulose acetate nanofibres: the present status and gamut of biotechnological applications. Bio-technol Adv, 31(4), 421-437.

[72] Evans, E. H. An Introduction to Analytical Atomic Spectrometry. Chichester: John Wiley & Sons Ltd; (1998); pp164-175.

[73] Gaydon, A. G., Wolfhard, H. G. Flames: Their Structure, Radiation and Temperature, London: Chapman & Hall; 1960; p. 304.

[74] Juza, J. (1997). The pendant drop method of surface tension measurement: equation interpolating the shape factor tables for several selected planes. Czechoslovak J Phys, 47(3), 351-357.

[75] Murray, H. H. (1991). Some application of clay minerals. Appl Clay Sci, 5, 379-395.

[76] Espinoza, D. N., Santamarina, J. C. (2012). Clay interaction with liquid and supercritical CO_2: The relevance of electrical and capillary forces. Int J Greenhouse Gas Control 10, 351-362.

[77] Bendou, S., Amrani, M. (2014). Effect of hydrochloric acid on the structural of sodic-bentonite clay. J Minerals & Mater Character & Eng 2, 404-413.

[78] Yildiz, N., Sarikaya, Y., Calimli, A. (1999). The effect of the electrolyte concentration, pH on the rheological properties of the original and the Na_2CO_3 -activated Kutahya bentonite. Appl Clay Sci 14, 319-327.

[79] Volzone, C., Garrido, L. B. (1991). The effect of some physico-chemical and mineralogical properties on the Na_2CO_3 activation of Argentine bentonites. Appl Clay Sci 6, 143-154.

[80] Pramanik, S., Das, G., Karak, N. (2013). Facile preparation of polyaniline nanofibres modified bentonite nanohybrid for gas sensor application. RSC Adv, 3, 4574-4581.

[81] Kumar, A. S., Mahto, V., Sharma, V. (2003). Behaviour of organic polymers on the rheological properties of Indian bentonite-water based drilling fluid system and its effect on formation damage. Indian J Chem Technol, 10, 525-530.

[82] Masindi, V. (2017). Application of cryptocrystalline magnesite-bentonite clay hybrid for defluoridation of underground water resources: implication for point of use treatment. J Water Reuse & Desalin 7, 338-352.

[83] Ghorani, B., Goswami, P., Russell, S. J. (2015). Parametric study of electrospun cellulose acetate in relation to fibre diameter. Res J Tex & Apparel 19(4), 24-40.

[84] Sebastiani, E., Lacquaniti, L. (1967). Acetic acid-water system thermodynamically correlation of vapour-liquid equilibrium data. Chem Eng Sci, 22, 1155-l 162.

[85] Demir, M. M., Yilgor, I., Yilgor, E., Erman, B. (2002). Electrospinning of polyurethane fibres. Polymer, 43, 3303-3309.

[86] Vega, C., De Miguel, E. (2007). Surface tension of the most popular models of water by using the test-area simulation method. J Chem Phys 126, 154707-154710.

[87] Hong, C. H., Ki, S. J., Jeon, J. H., Che, H. L., Park, I. K., Kee, C. D., Oh, I. K. (2013). Electroactive bio-composite actuators based on cellulose acetate nanofibres with specially chopped polyaniline nanoparticles through electrospinning. Compos Sci & Technol 87, 135-141.

[88] Theng, B. K. G., Greenland, D. J., Quirk, J. P. (1967). Adsorption of alkylammonium cations by mont-morillonite. Clay Minerals 7, 1-17.

[89] Qin, X., Hui, Wang. H., Wu, S. (2011). Investigation on structure and thermal properties of electrospun cellulose diacetate nanofibres. J Industrial Tex 42(3), 244-255.

[90] Zhang, J., Wilkie, C. A. (2005). Fire retardancy of polyethylene alumina trihydrate containing clay as a synergist. Polym Adv Technol 16(7), 549-553.

[91] Abdou, M. I., Al-sabagh, A. M., Dardir, M. M. (2013). Evaluation of Egyptian bentonite and nano-bentonite as drilling mud. Egyptian J Petroleum, 22, 53-59.

[92] VanderHart, D. L., Hyatt, J. A., Atalla, R. H., Tirumalai, V. C. (1996). Solid-state ^{13}C NMR and Raman studies of cellulose

triacetate: oligomers, polymorphism, and inferences about chain polarity. Macromolecules 29, 730-739.

[93] Zahedi, P., Rafie, A., Wojczak, E. (2016). Morphological and thermal properties of optimised electrospun cellulose acetate nanofibres during deacetylation in different pH values. Indian J Fibre & Tex Res 41, 13-18.

[94] Aouat, Y., Marom, G., Avnir, D., Gelman, V., Shter, G. E., Grader, G. S. (2013). Organically doped silver nanoparticles deposited on Titania nanofibers: enhanced catalytic methanol oxidation. J Phys Chem C, 117, 22325-22330.

[95] Tepper, F., Rivkin, T. (2002). Novel nanofibre filter medium attracts waterborne pathogens. Filtration & Separation, 39, 16-19.

[96] Paulsen, F. G., Shojaie, S. S., Krantz, W. B. (1994). Effect of evaporation step on macro void formation in wet-cast polymeric membranes. J Membrane Sci 91, 265-282.

[97] Ke, X. B., Zhu, H.Y., Gao, X. P., Liu, J. W., Zheng, Z. F. (2007). High-performance ceramic membranes with a separation layer of metal oxide nanofibers. Adv Mater, 19, 785-790.

[98] Guillen, G. R., Farrell, T. P., Kaner, R. B., Hoek, E. M. V. (2010). Pore structure, hydrophilicity, and particle filtration characteristics of polyaniline–polysulfone ultrafiltration membranes. J Mater Chem 20, 4621-4628.

[99] Zhu, H. Y. (2008). High-flux ceramic membranes with a nanomesh of metal oxide nanofibres. J Phys Chemist B, 112, 5000-5006.

[100] Ma, H., Chu, B., Hsiao, B. S. Functional nanofibres for water purification. In: Wei, Q. Editor, Functional nanofibres and their applications, Cambridge: Woodhead publishing Ltd; 2012; PP 331-370.

KD